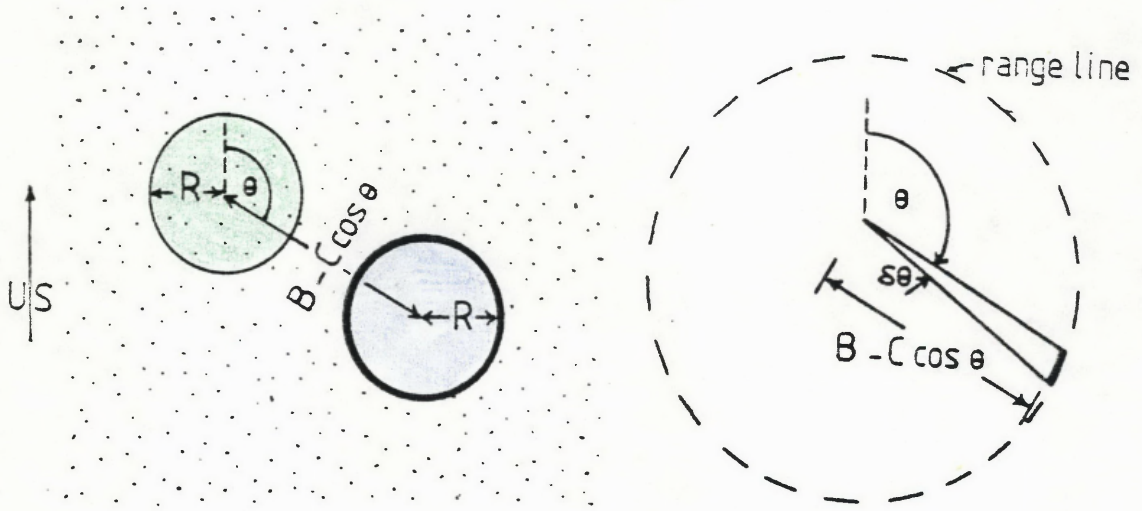

FIGURE 5.17: *Contributing region (green shading) for a circular sampling aperture of radius R, 2R < B - C. Source area, stippled; collecting area, blue shading.*

This inverse correspondence extends to the case where the sampling aperture is greater than the smallest particle displacement. As for the splash cup (Section 5.2.1, Figure 5.1), the contributing region is defined by the overlap of two circles - this is shown in Figure 5.18. The area of the contributing region is found in the same way as for the splash cup and can therefore be obtained by replacing B in equation (5.2) by B - Ccosθ to give:

$$2R^2 \sin^{-1} \frac{B - C\cos\theta}{2R} + B \sqrt{R^2 - \frac{(B - C\cos\theta)^2}{4}} .$$

The collecting rate, c_{12}, is:

$$c_{12} = \frac{im}{2\pi} \int_0^{2\pi} 2R^2 \sin^{-1} \frac{B - C\cos\theta}{2R} + B \sqrt{R^2 - \frac{(B - C\cos\theta)^2}{4}}$$

This can only be evaluated numerically - using Simpson's rule gives:

$$c_{12} = \frac{im}{6} \left[(B - C) \sqrt{R^2 - \frac{(B - C)^2}{4}} + 2R^2 \sin^{-1} \frac{B - C}{2R} \right.$$

$$+ 4B \sqrt{R^2 - B^2/4} + 8R^2 \sin^{-1} \frac{B}{2R}$$

$$\left. + (B + C) \sqrt{R^2 - \frac{(B + C)^2}{4}} + 2R^2 \sin^{-1} \frac{B + C}{2R} \right] , \qquad (5.18)$$

which bears no direct relationship to the component or resultant splash transport rates on the undisturbed part of the soil surface, or to the detachment rate.

Analysis of the Field Splash Cup

The vertical divisions of the field splash cup as used by Morgan (1982) are 10 cm high. For vertical distributions of splash such as those

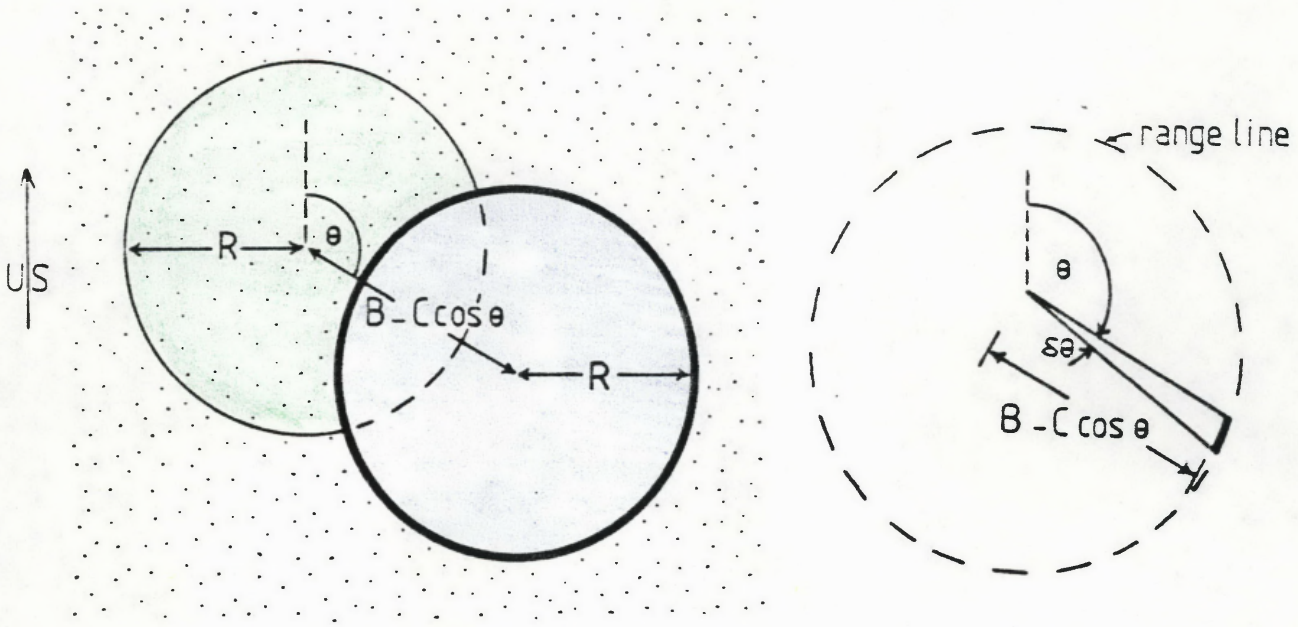

FIGURE 5.18: *Contributing region (green shading) for a circular sampling aperture of radius, R, 2R > B + C. Source area, stippled; collecting area, blue shading.*

recorded by Walker *et al.* (1978), boundaries of this height would allow the passage of some splashed particles, but prevent the passage of others. If only that part of the splash transport that is capable of passing over the 10 cm high vertical boundaries is considered, then the configuration can be regarded as a more complicated version of the previous configuration analysed, *i.e.* an annular sampling aperture rather than a circular one. The results of the previous analysis also apply, *viz.* if the diameter of the outer circle of the annulus is less than the shortest particle displacement, then, and only then, will the collection rate of the annulus be directly related to a process rate on the soil surface - in this case the detachment rate.

For those splash displacements to which the vertical divisions present a barrier, and for those greater in length than the diameter of the central source area, the collection rate by the upslope annulus can be obtained by first considering the contributing region for displacements whose directions lie in the range $0 \leqslant \theta \leqslant \pi/2$. This is shown in Figure 5.19(a). The area of a segment subtended by angle γ in a circle of radius r is (Spiegel, 1968):

$$\tfrac{1}{2}r^2 \, (\gamma - \sin\gamma) \, .$$

From the simple geometry shown in Figure 5.19(b), the subtending angle is 2θ, so that the area of the contributing region is:

$$\pi R^2 - \tfrac{1}{2}R^2 \, (2\theta - \sin 2\theta) \, .$$

The collecting rate in the upslope annulus for θ: $0 \leqslant \theta \leqslant \pi/2$ is given by the integral, I_1:

$$I_1 = \frac{im}{2\pi} \int_0^{\pi/2} \pi R^2 - \tfrac{1}{2}R^2(2\theta - \sin\theta) d\theta$$

$$= \frac{3im\pi R^2}{16} + \frac{imR^2}{4\pi} \, .$$

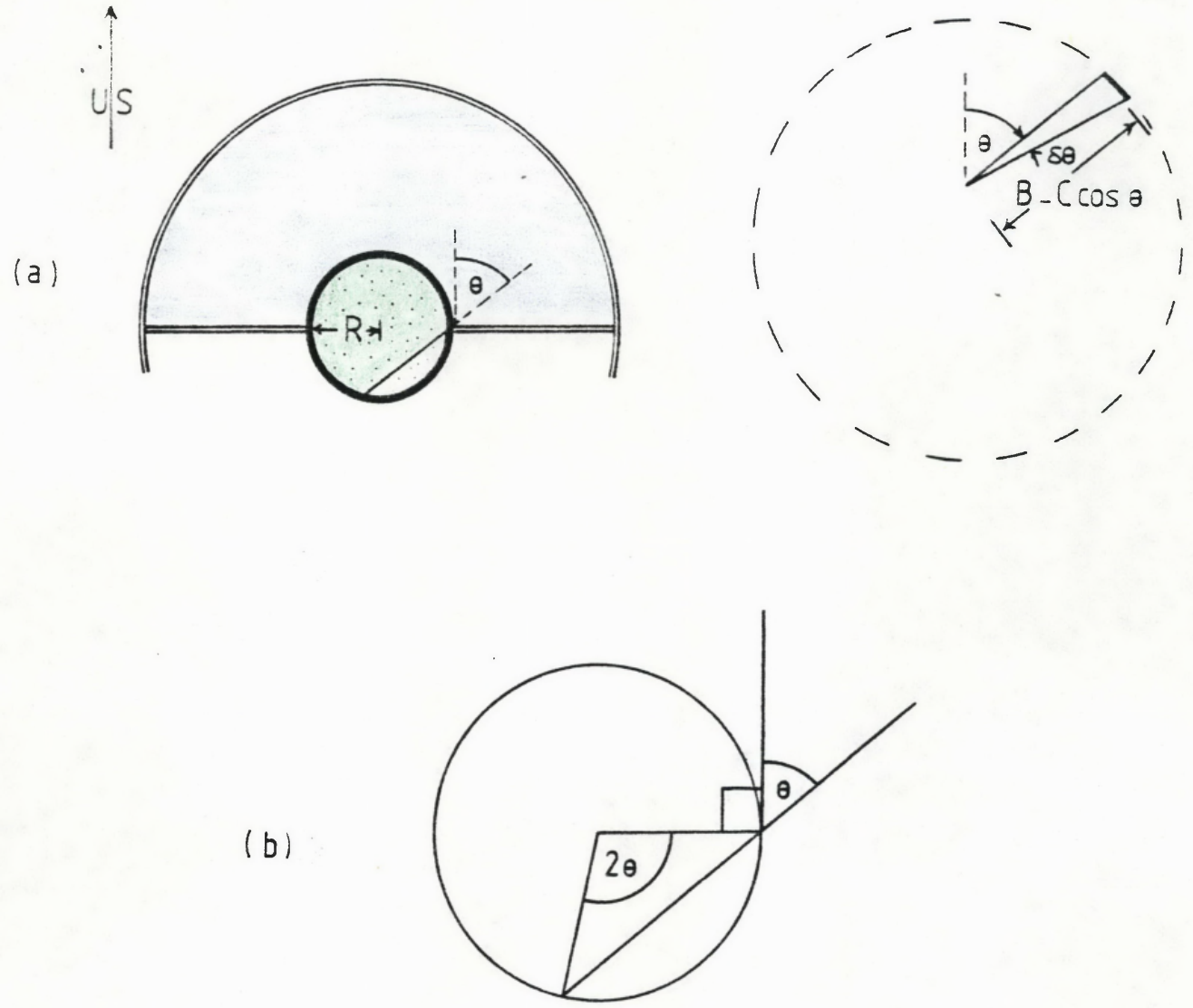

FIGURE 5.19: *a) Contributing region (green shading) for field splash cup; $0 \leq \theta \leq \pi/2$, $2R < B - C$, vertical divisions preventing the passage of splash. Source area, stippled; collecting area, blue shading.*
b) Subtending angle of 2θ for the chord separating the contributing region from the non-contributing region on the central source area.

It is necessary to consider also displacements with θ: $\pi/2 \leqslant \theta \leqslant \pi$ as these can also make some contribution to the upslope collecting annulus. The contributing region for such displacements is shown in Figure 5.20(a), and has an area of:

$$\tfrac{1}{2}R^2 \left[2\pi - 2\theta - \sin(2\pi - 2\theta)\right] ,$$

(Figure 5.20(b); Spiegel, 1968). The collecting rate for the upslope annulus for θ: $\pi/2 \leqslant \theta \leqslant \pi$ is given by the integral, I_2:

$$I_2 = \frac{im}{2\pi} \int_{\pi/2}^{\pi} \tfrac{1}{2}R^2[2\pi - 2\theta - \sin(2\pi - 2\theta)]d\theta$$

$$= \frac{im\pi R^2}{4} - \frac{imR^2}{4} - \frac{imR^2}{4\pi} .$$

Utilising the symmetry of splash displacements about the upslope/downslope direction, the total collection rate, c_{13}, for all displacements capable of contributing to the upslope collecting annulus is:

$$c_{13} = \frac{7im\pi R^2}{8} - \frac{imR^2}{2} , \qquad (5.19)$$

which shows direct relationship only to the detachment rate.

To extend the analysis to those displacements of length less than the central source area diameter is considered unnecessary in the light of previous analysis. This has consistently shown that non-quadrilateral contributing regions with a maximum dimension greater than some or all of the particle displacements lead to an expression for the collecting rate which is complex and not directly related to component or resultant splash transport rates or to the detachment rate.

Given the above findings, the range of particle displacements likely to be encountered in the field, the 10 cm high vertical divisions and 10 cm

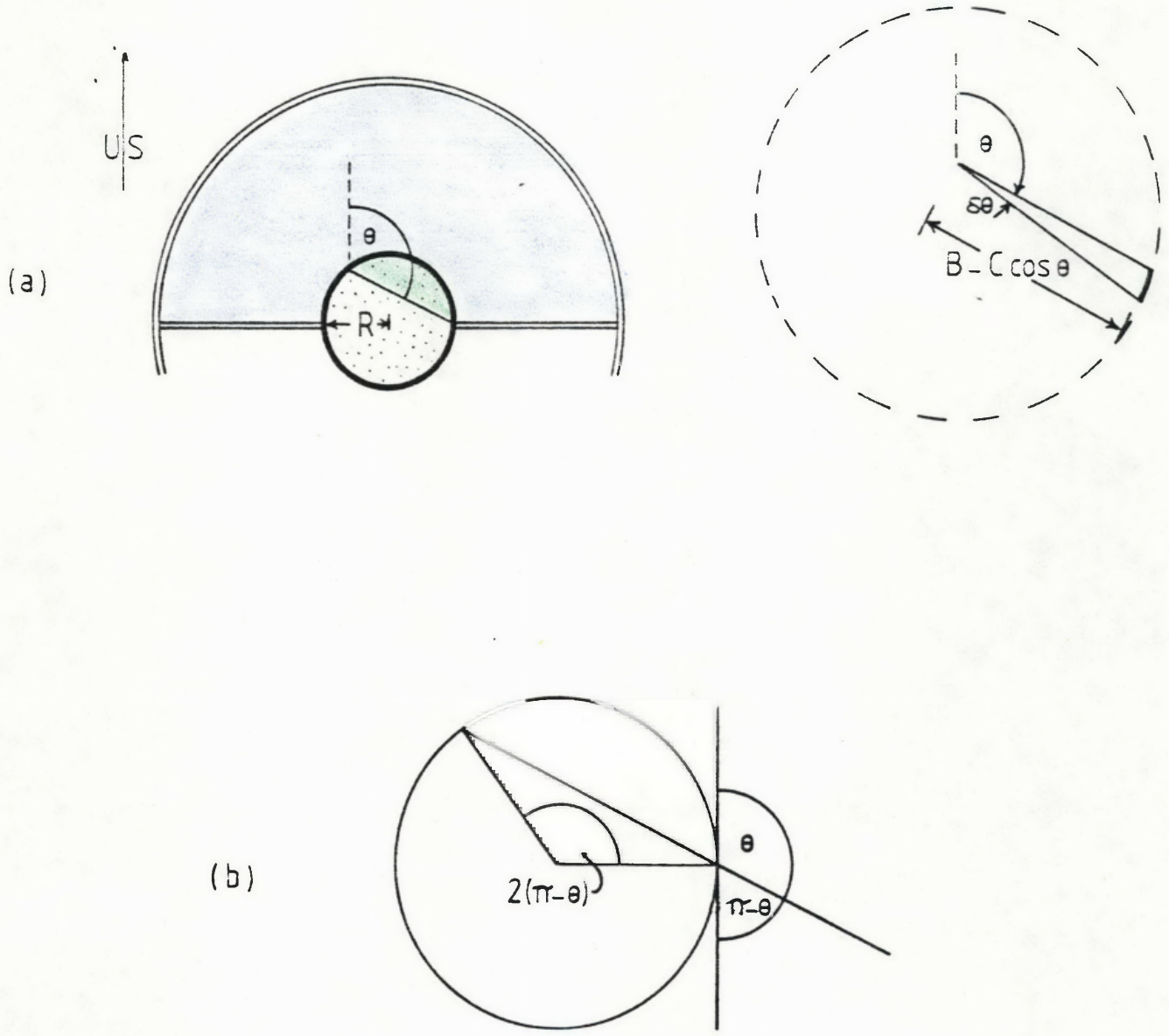

FIGURE 5.20: *a) Contributing region (green shading) for field splash cup; $\pi/2 \leq \theta \leq \pi$, $2R < B - C$, vertical divisions preventing passage of splash. Source area, stippled; collecting area, blue shading.*
b) Subtending angle of $2\pi - 2\theta$ for the chord separating the contributing region from the non-contributing region on the central source area.

diamter central source area used by Morgan, it is apparent that only for those particle displacements rising less than 10 cm from the surface and travelling more than 10 cm across the soil surface is there any useful relationship between the collecting rate in the annuli and process rates on the soil surface - in this case the detachment rate. As the configuration does not separate these particular displacements from others arriving in the collecting annulus, it can be expected that the overall collecting rate in either annulus would be unrelated to any process rates on the soil surface.

5.3.2 Tracer methods

The basic element of information obtained from tracer measurements is the post-event spatial distribution of marked or labelled soil in the region surrounding the pre-event point or line of application.

In the case of point application, the spatial distribution can be expressed as a density function in cylindrical coordinates:

$$T = t_\rho(r,\theta) \qquad 0 \leqslant r \leqslant f_t(\theta), \quad 0 \leqslant \theta \leqslant 2\pi$$

$$T = 0 \qquad r > f_t(\theta), \quad 0 \leqslant \theta \leqslant 2\pi$$

where T gives the mass of labelled particles present at a point situated at distance r in direction θ from the point of pre-event application. $f_t(\theta)$ is the equation of the line beyond which no labelled particles are found. If the size of the pre-event application of labelled particles is small compared to the expanse of the post-event distribution, then the r,θ coordinates are almost exactly equal to the distance and direction, respectively, that mass $t_\rho(r,\theta)$ was transported during the event.

The concept of component splash erosion put forward by Van Heerden (1964, 1967), and extended by this author to component inter-rill erosion (Section 4.3.3) is of use here also. Whereas in Section 4.3.3 component inter-rill erosion was applied to the distribution function $m(r,\theta)$ characterising the displacements due to one drop impact, here that which is termed component inter-rill event erosion is applied to the distribution function $t_\rho(r,\theta)$

characterising the labelled particle displacements due to the whole event. Thus the upslope component inter-rill event erosion, for example, can be written:

$$\int_{-\pi/2}^{\pi/2} \cos\theta \int_{0}^{f_t(\theta)} t_\rho(r,\theta) \cdot r^2 \, dr \, d\theta \, ,$$

and, in exactly the same way as in Sections 4.3.2 and 4.3.3 it can be shown to be equal to the upslope component inter-rill event transport. This is the mass of soil that crossed during the event from the downslope side to the upslope side of unit length of a line oriented cross-slope on the soil surface. Thus the distribution $t_\rho(r,\theta)$ defined by tracer measurements can be used to determine the components and resultant of the soil transport that took place during the event. This would preferably be done by discrete methods as measurements of marked particle concentration would be at a finite number of points.

For the case where marked soil is applied in a narrow band across slope, two dimensional analysis will suffice, provided certain conditions pertaining to end effects are met. Firstly, consider a band of marked soil as shown in Figure 5.21(a). The dashed curve shows the patial limit of marked particles found post-event. Clearly, distances a and b between the ends of the marked band (A and D respectively, Figure 5.21(a)) and the post-event marked particle limit, represent the maximum distance of cross-slope transport, to left and right respectively. The concentration of marked particles in the areas upslope and downslope of sections AB and CD of the marked soil band could therefore be expected to be affected by the termination of the marker band at A and D respectively. Only on the region of the soil surface upslope and downslope of section BC is the marked particle concentration free of end effects. The concentration of marked particles along line EF through this region is shown in Figure 5.21(b). Note that a marked particle on line EF at distance x from G on the marked soil band has an upslope or downslope *component* of displacement of x, *i.e.* its actual point of origin on the marked soil band, and therefore its direction of displacement is not specified. If the distribution shown in Figure 5.21(b) is denoted $t_b(x)$, and the width of the marked soil band is narrow compared to the spatial

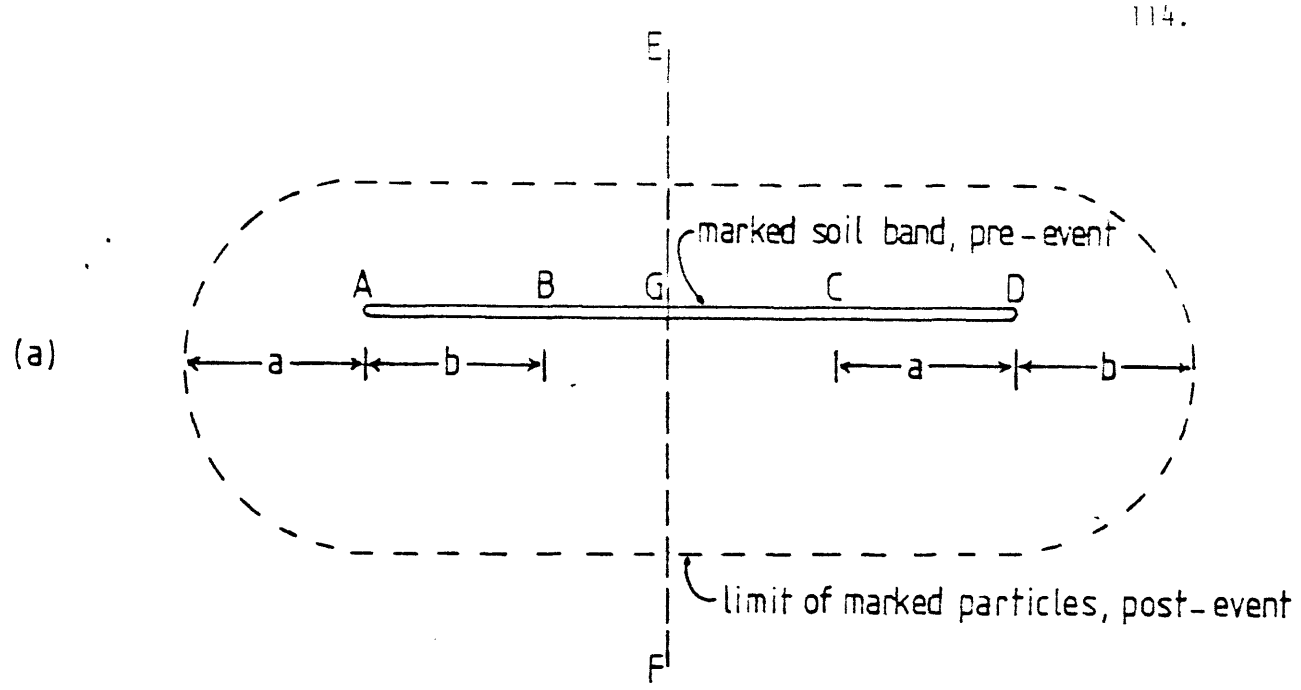

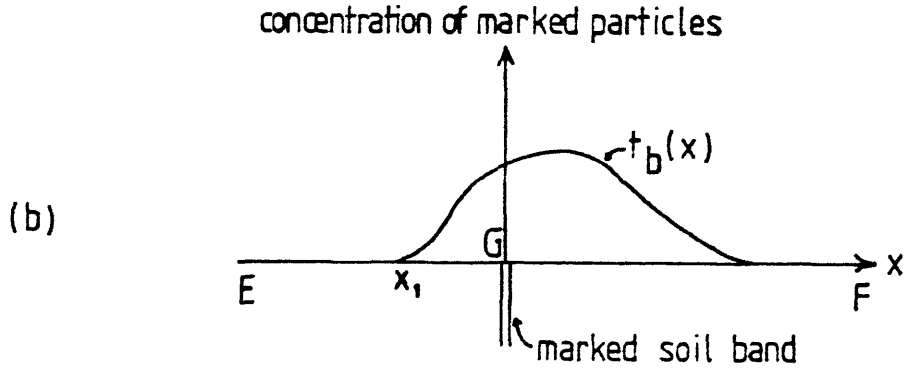

FIGURE 5.21: *a) Plan view of hypothetical pre-event marked soil band and post-event spatial limit of marked particles.*
b) Marked particle concentration versus distance from marked soil band along line EF.

expanse of $t_b(x)$, then forming the expression:

$$\int_0^{x_1} x \cdot t_b(x)\, dx$$

gives the upslope component inter-rill event erosion, which has already been shown to be equal to the upslope component inter-rill event transport rate.

Thus it has been shown that, given a measured post-event distribution of marked particles about the pre-event application of marked soil particles at a point or in a narrow band, it is possible to calculate the upslope or downslope component inter-rill transport for the event. The analysis presented assumes that there are marked particles at the site of pre-event placement available for transport throughout the event. As a result, the method cannot apply to depositional sites, or to sites where the depth of removal of soil exceeds the depth of placement of the marked soil.

5.4 Application of Full Analysis to Source/Collecting Area Configurations

With the exception of tracer methods dealt with in the previous section, all the measurement methods discussed have involved source/collecting area configurations, which have been analysed using the simplified representation of the inter-rill transport process developed in Section 4.2. This has the advantage that most of the integral expressions obtained could be evaluated to yield simple expressions in terms of i, the drop impact rate, m, the mass splashed by each drop and B and C the drop impact variables defined by equations (4.5) and (4.6) respectively. Full analysis involving both splash and flow displacements, on the other hand, results in double integral expressions that cannot, in general, be evaluated (Section 4.3). Nevertheless, it is possible to show that the conclusions reached pertaining to the simplified representation (Sections 5.2 and 5.3.1) also apply for the full analysis. Two examples are given - one where the collecting rate is directly related to a component transport rate, and one where such a relationship does not exist.

5.4.1 Full analysis of single boundary configuration type 3

As for the simplified representation, first consider just one direction, θ, and magnitude, r, of displacement from the total set of displacements for one drop impact specified by the distribution function $m(r,\theta)$. The contributing region for one such direction and magnitude of displacement is shown in Figure 5.22. The area of this region is:

$$\text{length EF} \times \text{length FG} = b \times -r\cos\theta$$

$$= -br\cos\theta \ .$$

The mass displaced distance r in direction θ is $r\delta\theta\delta r$ (Section 4.3.2). For a drop impact frequency of i, the collecting rate for displacements of length r in direction θ is:

$$i \cdot b \cdot m(r,\theta) \cdot r^2 \cdot \cos\theta \cdot \delta r \cdot \delta\theta \ .$$

The total collecting rate, c_{14}, for all displacements capable of reaching the collecting area is:

$$c_{14} = -i\ b \int_{\pi/2}^{3\pi/2} \cos\theta \int_{0}^{f(\theta)} m(r,\theta) \cdot r^2 \ dr \ d\theta$$

$$= -i \int_{\pi/2}^{3\pi/2} \cos\theta \int_{0}^{f(\theta)} m(r,\theta) \cdot r^2 \ dr \ d\theta \quad \text{per unit width of same area ,} \qquad (5.20)$$

which is identical with the corresponding field downslope component inter-rill transport rate (equation (4.24). The restrictions on the source/collecting area configuration necessary for this identity to hold are the same as those

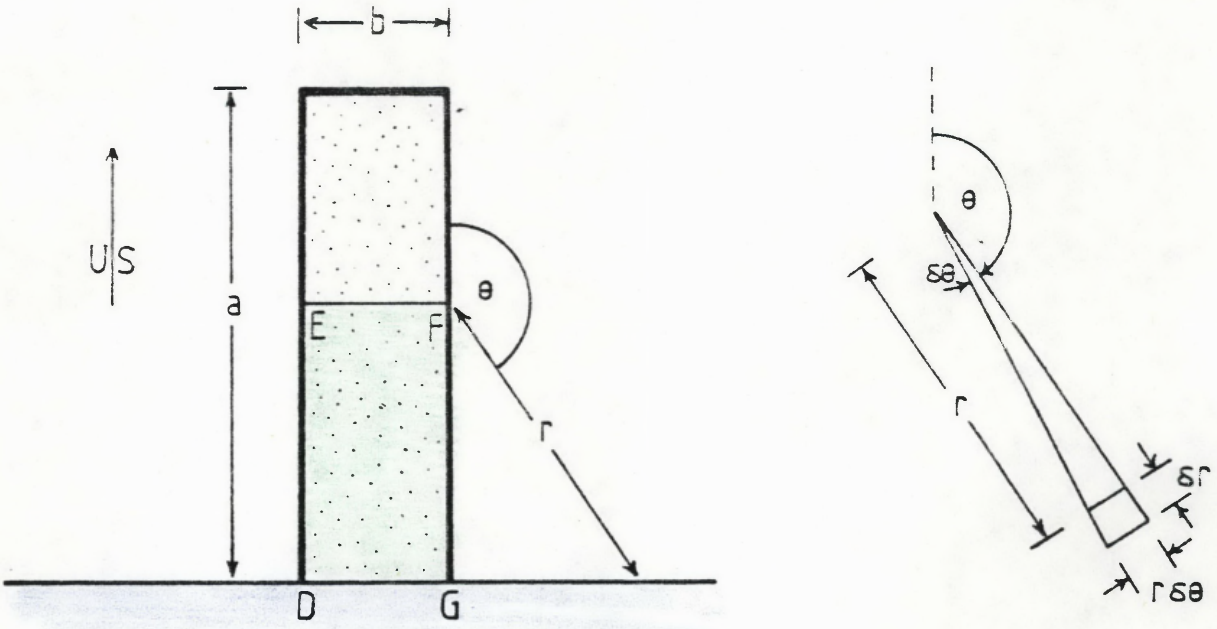

FIGURE 5.22: *Contributing region (green shading) for full analysis of single boundary configuration type 3. Source area, stippled; collecting area, blue shading.*

for the simplified representation (see p. 92). Note that the delineation of a contributing region, the derivation of its area, the derivation of an expression for the collecting rate for one direction or one direction and magnitude of displacement, and the extension by integrating to an expression for the collecting rate due to all displacements capable of reaching the collecting area is followed in both the simplified and the full analysis (compare Figure 5.10 and Figure 5.22 and the analyses leading to equations (5.14) and (5.20). The full analysis can be obtained from the simplified representation merely by the substitution of $m(r,\theta)$ for m and r for $B - C\cos\theta$, and formation of a double integral with appropriate transfer of limits.

5.4.2 Full analysis of total loss measurement

The parallels between the full analysis and the simplified representation noted above are here used to avoid duplication of analysis. In the section on the analysis of total loss measurement (p. 78), the total loss rate for the simplified representation is given in equation (5.9) as twice the sum of two integrals, I_1 (equation 5.7)) and I_2 (equation (5.8)). Making the appropriate substitutions, and forming double integrals, I_1 and I_2 become for the full analysis:

$$I_1 = ib \int_0^{\pi/2} \cos\theta \int_0^{f(\theta)} m(r,\theta) \cdot r^2 \, dr \, d\theta$$

$$+ ia \int_0^{\pi/2} \sin\theta \int_0^{f(\theta)} m(r,\theta) \cdot r^2 \, dr \, d\theta$$

$$- ib \int_0^{\pi/2} \cos\theta \sin\theta \int_0^{f(\theta)} m(r,\theta) \cdot r^3 \, dr \, d\theta \qquad (5.21)$$

$$I_2 = - ib \int_{\pi/2}^{\pi} \cos\theta \int_0^{f(\theta)} m(r,\theta)\cdot r^2 \, dr \, d\theta$$

$$+ ia \int_{\pi/2}^{\pi} \sin\theta \int_0^{f(\theta)} m(r,\theta)\cdot r^2 \, dr \, d\theta$$

$$+ ib \int_{\pi/2}^{\pi} \cos\theta \sin\theta \int_0^{f(\theta)} m(r,\theta)\cdot r^3 \, dr \, d\theta \, . \qquad (5.22)$$

The total loss rate, c_{15}, from the tray is given by:

$$c_{15} = 2(I_1 + I_2) \, , \qquad (5.23)$$

so that although this expression contains some terms related to component transport rates, it is not, due to the presence of terms containing $m(r,\theta)\cdot r^3$, directly related to either the total detachment rate given by:

$$\int_0^{2\pi} \int_0^{f(\theta)} m(r,\theta) dr \, d\theta \, ,$$

or to any of the component transport rates given by equations (4.21) to (4.25) or to the resultant transport rate given by equations (4.26) and (4.27).

Chapter 6

IMPLICATION OF ANALYSIS AND APPLICATIONS FOR EXPERIMENTAL PROGRAMME

6.1 Laboratory Measurement

6.1.1 Splash cups

It has been shown in Section 5.2.1 (Figure 5.2), that as the ejection velocity of splashed particles from the surface of a standard 8.9 cm splash cup decreases below 1.6 ms^{-1}, then a decreasing fraction of the total mass of particles detached from the surface falls outside the splash cup to be registered as mass loss from the cup. Ejection velocities have been measured as lying in the ranges of 0.5 ms^{-1} to 2.7 ms^{-1} (Levin and Hobbs, 1971) and 0.6 ms^{-1} to 3.0 ms^{-1} (Perrens and Reeve, 1982). A splash angle of 45° and an ejection velocity of 1.6 ms^{-1} corresponds to a range of 26 cm (neglecting air resistance). Published splash distributions (Mutchler, 1970; Reeve and Perrens, 1980) show that a significant proportion of splash is displaced less than 26 cm. Thus a significant proportion of splash detachment could have ejection velocities less than 1.6 ms^{-1}, and the standard splash cup could be expected to underestimate the total splash detachment. Obviously with smaller diameter splash cups, this underestimate becomes less significant, although at very small diameters, the number of drops striking the splash cup edges becomes a significant proportion of the total, which may also affect the fraction of the total detachment measured as loss from the cup.

A number of studies have used splash cups to investigate the effect of drop fall velocity or kinetic energy upon the splash loss from splash cups. These are summarised in Table 6.1. The data of Ellison (1944) have been omitted, since, as pointed out by Bisal (1960), Ellison's measurement of splash loss included a transportation factor as well as detachment. The table shows that the splash loss has generally been found to be proportional to the fall velocity to the power of 1.4 to 3.2 (mean 2.25).

TABLE 6.1: *Published relationships between splash loss (S) and drop fall velocity (V) or drop kinetic energy (ke)*

Author	Splash loss/ fall velocity relationship	Splash loss/ kinetic energy relationship
Mihara (1952)	$S \propto V^2$ *	$S \propto ke$
Free (1960)	$S_{sand} \propto V^{1.3}$ *	$S_{sand} \propto ke^{0.9}$
	$S_{soil} \propto V^{3.0}$*	$S_{soil} \propto ke^{1.5}$
Bisal (1960)	$S \propto V^{1.4}$	
Bubenzer and Jones (1971)	$S \propto V^{3.2}$ *	$S \propto ke^{1.6}$

* relationships calculated by this author from published kinetic energy relationship.

The relationship betweem P, the fraction of total detachment collected outside the cup, and the ejection velocity, v, given for various values of splash angle, α, in Figure 5.2 can be expressed as power curves, *viz.*:

$\alpha = 10°, 80°$ $\quad P = .4618\ v^{1.916}$ $\quad (r = .999)$

$\alpha = 30°, 60°$ $\quad P = 1.1005\ v^{1.893}$ $\quad (r = .998)$

$\alpha = 45°$ $\quad P = 1.1609\ v^{1.803}$ $\quad (r = .996)$.

If the assumption is made that the ejection velocity, v, is more or less linearly related to the drop fall velocity, V (there is no published evidence to support or discount this), then the above power curves could be replaced by:

$$P \overset{\text{approx.}}{\propto} V^{1.86}, \quad \text{for the normal range of } \alpha,$$

i.e. for constant total detachment, the fraction of this collected outside the cup is itself proportional to the fall velocity to the 1.86 power (or some other power if the assumption of linearity above is not strictly correct). This suggests that some or all of the variation of splash loss with drop fall velocity or kinetic energy found by the authors listed in Table 6.1 could be in fact due to the variation in the fraction collected rather than in the total detachment.

Given the fundamental importance of detachment/kinetic energy relationships derived from splash cup studies in deterministic modelling and predictive techniques (see, for example, column 3 of Table 2.3), this area was felt to be worthy of further study. A preliminary investigation into the effects of splash cup diameter on measured detachment was undertaken. The results are given in Section 8.1.

6.1.2 Soil trays

In the section on qualitative considerations (p. 74), it was shown that the distribution of inter-rill transport rates on a rectangle of soil in isolation, as in a laboratory soil tray, is entirely different to that which prevails in the same rectangle under the same conditions in the field surrounded by an expanse of similar soil. This phenomenon cannot be avoided by faithful simulation of field conditions in the laboratory - it is an inevitable consequence inherent in transport by omni-directional particle displacements. Figure 5.4 shows that the distribution of resultant transport rates on a sloping rectangular soil tray can be expected to consist of an inner zone where resultant transport rates are the same as that which would prevail were the rectangle sited back in the field, and a peripheral zone where this does not apply. The width of the peripheral zone is equal to the greatest length of particle displacement, since at points further than this from the tray boundary, the transport process is no longer affected by the lack of soil outside the tray boundary. Thus the peripheral zone may be at least one metre in width, so that only in the case of very large soil trays (at least greater than 2 m square) will there be an inner zone where the resultant transport rate is unaffected by the tray boundary. The majority of published configurations have a source area less than 2 m square and therefore do not have the unaffected inner zone, *i.e. nowhere on trays of this size is*

the resultant transport rate the same as it would be were the rectangle of soil in the tray returned to the field

The analysis presented above (pp. 78-99) shows that, despite this discouraging characteristic of small soil trays, several specific source/collecting area configurations have collecting rates that are directly related, *not to any of the resultant transport rates on the soil tray, but to the resultant transport rate that would prevail were the rectangle of soil surrounded by an expanse of similar soil, as it would be in the field.* Other source/collecting area configurations were shown to have collecting rates directly related to the detachment rate on the soil surface. The source/collecting area configurations that have a collecting rate directly related to a transport or detachment rate are shown in Figure 6.1. The dimensional restrictions upon the validity of such relationships are also show in this figure.

These restrictions are particularly significant when it comes to translating the theoretically justified configurations of Figure 6.1 into practical experimental designs. The configuration for the measurement of detachment rate carries the proviso that the maximum dimension of the source area be less than the minimum soil particle displacement. As particle displacements range in size from zero upwards, the best estimate is therefore to be obtained by having the source area as small as possible, consistent with realistic soil conditions and with keeping the number of drops striking the source area edge a suitably small fraction of the total.

As discussed in Section 3.5, boundary effects determine to which of the inter-rill transport processes the configurations of Figure 6.1 can be applied. Despite the fact that these configurations will provide direct relationships between collecting rates and component inter-rill transport rates, the difficulties associated with boundaries when flow transport is occurring make it expedient to confine the application of these configurations to the splash transport process.

Of the two configurations for the measurement of component transport rates, that involving the smaller source area was chosen for reasons of weight of soil involved and of practical convenience. The feasibility of measuring by this means the net downslope component splash transport was

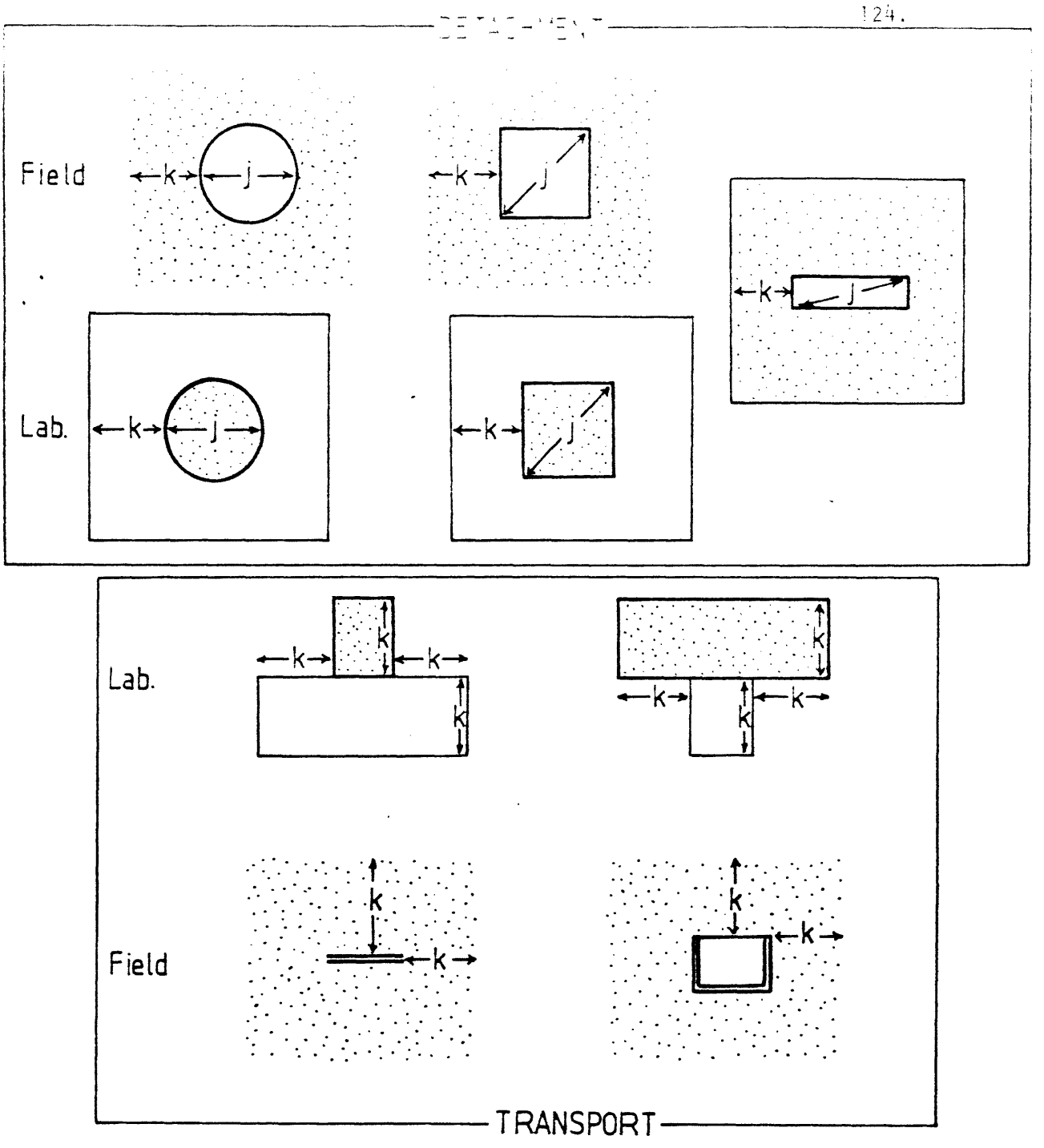

FIGURE 6.1: *Source/collecting area configurations for which the collecting rate is equal to the detachment rate or a component transport rate, provided j is less than the smallest particle displacement and dimension k is greater than the largest particle displacement. Outer collecting area boundaries in laboratory configurations could be replaced with boundaries over which transport cannot take place, in which case k would cease to be a critical dimension. Source area, stippled; collecting area, plain; boundary over which transport can take place, single line; boundary over which transport cannot take place, double line.*

tested in a study undertaken by Mr Alan Bush and reported in Bush (1981). The results of this study are given in Section 8.2.

6.2 Field Measurement

6.2.1 Splash traps

In the section on qualitative considerations (p.101), it was shown that splash traps must inevitably cause some distortion to the resultant transport rates in their vicinity. A vertical intercepting surface was shown to collect splash at rates directly related to the undisturbed component transport rates on the soil surface, despite the disturbance in the vicinity of the intercepting surface (see section on Analysis of Vertical Intercepting Surfaces, p.101). No dimensional restrictions were found to be necessary for this configuration.

The collecting rate for sampling apertures flush with the soil surface, however, was found equal to the detachment rate on the soil surface only if the maximum dimension of the aperture was less than the shortest particle displacement. So, as for the soil tray, the best estimate of detachment rate is obtained when the sampling aperture is as small as possible, consistent with keeping the number of impacts at the edge of the aperture a suitably small fraction of the total number capable of contributing splash into the aperture. The field splash cup was found to have a very narrow range of particle displacements for which a valid estimate of detachment rate is obtained from its collecting rate and was therefore dismissed as a possible measurement method. The acceptable field configurations are shown in Figure 6.1 with the laboratory configurations.

Since the analysis of vertical intercepting surfaces (p.101) applies equally to a vertical sampling aperture (*i.e.* the analysis holds regardless of how splashed particles are gathered once having intercepted or passed through a vertical plane), a splash trap design embodying this was developed. As the concept owes much to the splash traps first used by Bollinne, the new design is termed the modified Bollinne splash trap. It is illustrated as a source/collecting area configuration in Figure 6.1 and described in detail in Section 7.3. The practicality of the design was tested in field installations

and results are given in Section 8.3. A splash board design was also tested in the field and results for this are given in Section 8.3.

6.2.2 Tracer methods

It has been shown in Section 5.3.2, that the post-event distribution of marked particles can be used to determine: (i) the resultant and component inter-rill transport when pre-event point application is used; (ii) two components of inter-rill transport at right angles to the marked band when pre-event strip application is used. The tracer method is notable among the methods examined in its absence of boundary problems and this is a major point in its favour. There are, however, practical disadvantages. The most obvious is that once the measurement site has been contaminated by the transport and dispersion of marked particles, it is no longer usable, unless the nature of marking is changed or the marked particles lose their distinguishing characteristic. As it was felt that experience with a tracer method would be a useful adjunct, both as an absolute "boundary-effect-free" method of measurement and to lend depth to the overall assessment of inter-rill transport measurement methods, a simple tracer method was tested. Results are given in Section 8.4.

Chapter 7

METHODS OF EXPERIMENTAL PROGRAMME

7.1 Splash Cup Study

7.1.1 Sand

A clean quartzose river sand with sub-angular to sub-rounded grains was used. The size grading is given in Table 7.1.

7.1.2 Splash cups

Three cylindrical splash cups of diameters 3.1, 9.0 and 15.3 cm and height 5.0 cm were used. The 3.1 cm diameter splash cup was fabricated using a section of black polythene pipe with a galvanised sheet metal base, while the other two were wholly of sheet metal. The cups were not provided with drainage.

7.1.3 Drops

Single water drops of 5.6 and 4.7 mm equivalent spherical diameter were produced by a cloth and a wool dropper respectively. Water was fed to the dropper from a reservoir via a constant head tank (to give a constant drop rate), through a solenoid valve (for remote control from the working area) and through a filter (Plate 7.1). The dropper was mounted 9.75 m above the working area and drops fell within a vertical 9 m length of 90 mm p.v.c. pipe. Rainwater was considered as sufficiently pure for use with the non-cohesive sand.

7.1.4 Procedure

Splash cups were filled to level with the rim with sand and rainwater added until the capillary fringe was just visible at the surface, *i.e.* the sand was fully saturated but with no ponded water. This condition was chosen as it is easily duplicated merely by observation. Single drops were applied randomly and as uniformly as possible over the sand surface by moving the splash cup slightly between drops. As the two drop sizes used showed only

TABLE 7.1: *Size grading of sand used in splash cup study*

Sieve aperture (mm)	Percentage passing
4.750	100.00
2.360	98.39
1.180	72.00
0.625	27.43
0.425	11.11
0.300	3.05
0.150	0.07
0.075	0.04

slight drift during their descent, it was possible with the two larger size splash cups to avoid drop impacts on the splash cup rim. With the smallest splash cup, however, this was not possible. Measurements were discarded when the drop impact occurred on the splash cup rim.

The number of drops applied to each cup was calculated so that each had the same number of impacts per unit of surface area, *viz.* 3.1 cm cup - 1 drop, 9.0 cm cup - 8 drops, 15.3 cm cup - 23 drops. After this number of drops, a fresh surface was exposed by replacing the sand in the cup. As the variability in measurements of the splash detachment is a function of the number of drops in the measurement, the procedure was repeated so that the total number of drops used in each measurement was nearly the same. Thus: 3.1 cm cup - 23 runs; 9.0 cm cup - 3 runs; 15.3 cm cup - 1 run. Splash was collected in a larger cylindrical container in which the splash cup was placed. The splashed sand from all the runs for a given cup size/drop size measurement was accumulated in the container, then removed, oven-dried and weighed. Each measurement of detachment for a given cup size/drop size combination was made in duplicate.

7.1.5 Calculations

The kinetic energy of the falling drops was calculated using the fall velocity values of Mutchler (1970) who used the same drop fall of 9.75 m and similar size drops to those used in this study.

7.2 Soil Tray Study

A brief description of the methods used is given here - full description is given in Bush (1981). Two soils were used, both black earths from the N.S.W. Soil Conservation Service Research Station plots at Gunnedah - one from a stubble burnt plot and one from a stubble mulched plot. The study employed a single boundary type 3 configuration at the upslope and downslope ends of a 100 cm × 30 cm soil tray. The arrangement of source and collecting areas is shown in Figure 7.1. The soil was air-dry at the commencement of application of simulated rainfall from a Morin-type rotating disc simulator. Rainfall was applied at 105 mh^{-1} for 10 minutes. The water/soil mixture splashed into the collecting trays was filtered and the soil oven-dried and weighed. The mass in trays 1 and 2 (Figure 7.1) gives the upslope component splash transport per 30 cm source width, while that in trays 5 and 6 gives the downslope component splash transport per 30 cm source width. The total loss, *i.e.* the mass in trays 1 to 6 was also measured.

7.3 Splash Trap Study

7.3.1 Soil and plot

The splash traps were sited on a sandy loam of the Woolshed Series at the Newholme Field Laboratory. The size grading of the soil is given in Table 7.2. The plot is situated on a south-southeast facing slope on the southern flank of Mt Duval, with a clear exposure to the southwest and some shelter from trees and a building to the east. The plot was prepared by chisel-ploughing and harrowing several months before the splash traps were installed. It has subsequently been kept in bare fallow condition with a rotary tiller. The plot was tilled at approximately three monthly intervals and carefully raked by hand after each erosion event to maintain a uniform sloping surface. The plot has a 17.6% slope with downslope and upslope

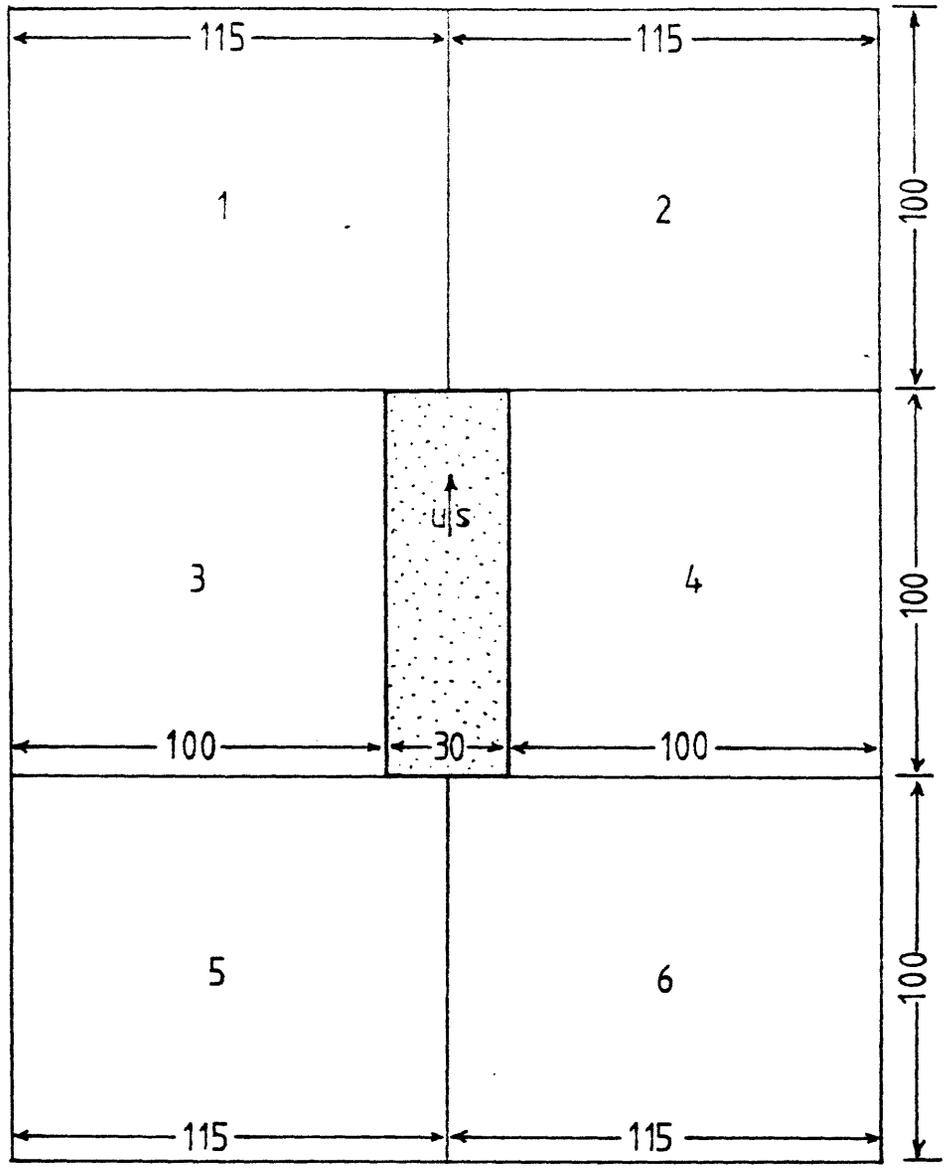

FIGURE 7.1: *Source/collecting area configuration used in soild tray study. Collecting trays are numbered 1-6. Source area, stippled; all dimensions in cm.*

TABLE 7.2: *Size grading of sandy loam (Woolshed Series) from splash erosion plot at Newholme Field Laboratory*

Sieve aperture (mm)	Percentage passing
2.360	100.00
1.180	92.35
0.625	69.93
0.425	56.35
0.300	47.00
0.150	27.40
0.075	14.75

directions being 164.5° and 344.5° east of north respectively. A diversion channel at the top end of the plot excludes runoff from above the plot.

7.3.2 Splash traps

The prototype splash traps first used were of two types: (i) a vertical intercepting surface modelled after the splash boards of Ellison (1944); (ii) a vertical sampling aperture termed the modified Bollinne splash trap. The final design used was a narrow vertical sampling aperture termed the pipe splash trap after its constructional basis.

The splash boards were fabricated of galvanised sheet metal to provide a vertical intercepting surface 30 cm wide and 60 cm high (considerably higher than Ellison's design) bordered by a 2 cm wide trough on each side of the lower margin (Figure 7.2, Plate 7.2). In the manner of Ellison's design, the splash board was provided with a roof of width equal to the combined width of the troughs and the intercepting surface. The splash boards were held in place by two spikes at their base driven into the soil (Figure 7.2).

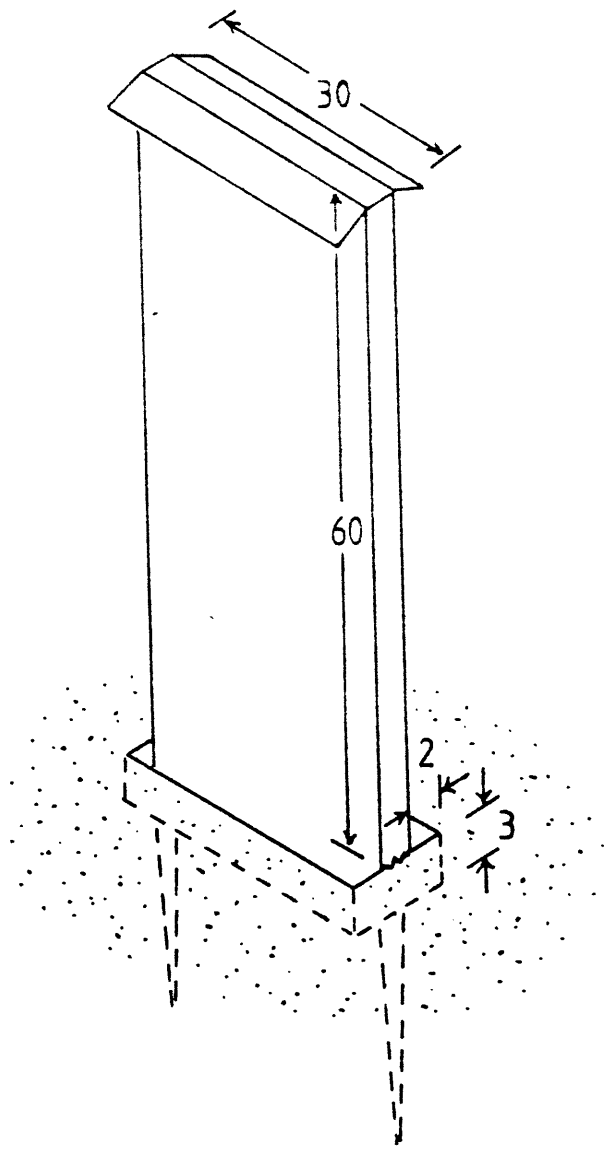

FIGURE 7.2: *Splash board. Dimensions in cm.*

PLATE 7.1: *Top of drop tower. Jerry-can reservoir and constant head tank partly obscured by R.S.J. at top of photograph. Filter and solenoid valve on wall at right.*

PLATE 7.2: *Splash board - dimensions given in Figure 7.2, preceding page.*

The modified Bollinne splash traps were fabricated of galvanised sheet metal in the form of a rectangular box 30 cm wide by 40 cm deep by 70 cm high with a 30 cm by 60 cm opening, the sampling aperture, in one of the 30 cm by 70 cm faces (Figure 7.3, Plate 7.3). The box was set 10 cm into the soil so that the lower edge of the opening was just above the soil surface. The roof of the box was constructed with a slight slope to direct water to the back of the trap away from the sampling aperture. The floor of the trap was furnished with a layer of metal gauze to minimise splashing out of the trap.

The pipe splash traps were constructed of a 103 cm length of 5 cm diameter p.v.c. pipe. A 3.1 cm wide opening was cut along 80 cm of the length of the pipe leaving 20 cm of uncut pipe to be set into the soil (Figure 7.4, Plate 7.4). End caps were fitted to both ends of the pipe to produce a splash trap with a 3.1 cm wide by 80 cm high sampling aperture. The edge of the aperture flush with the soil surface consisted of a sheet aluminium insert pop-rivetted to the pipe just below soil level. The splash traps were supported by wiring to a small steel stake driven into the soil diametrically opposite the sampling aperture.

7.3.3 Siting of splash traps

An array of two splash boards was sited with one splash board aligned across slope and one aligned up and down the slope so that upslope and downslope component splash transport rates would be measured by the former and the two cross-slope components by the latter. To avoid interference between the traps they were positioned 1.2 m apart. The modified Bollinne splash traps were sited in an array of three traps, one trap with its sampling aperture facing upslope, and the other two with sampling apertures facing outwards at 120° intervals. As there was no possibility of interference between traps with this arrangement, the backs of the traps were within 30 cm of each other. The seven pipe traps were divided into an array of four traps and an array of three traps. The four trap layout was based on a square array with one trap at each corner. The length of the side of the square was 1.2 m. The diagonals of the square were aligned across slope and up and down slope. The apertures of the traps faced to the centre of the square so that each trap measured one of: upslope; downslope, left and right cross-slope component splash transport. The three pipe trap array was

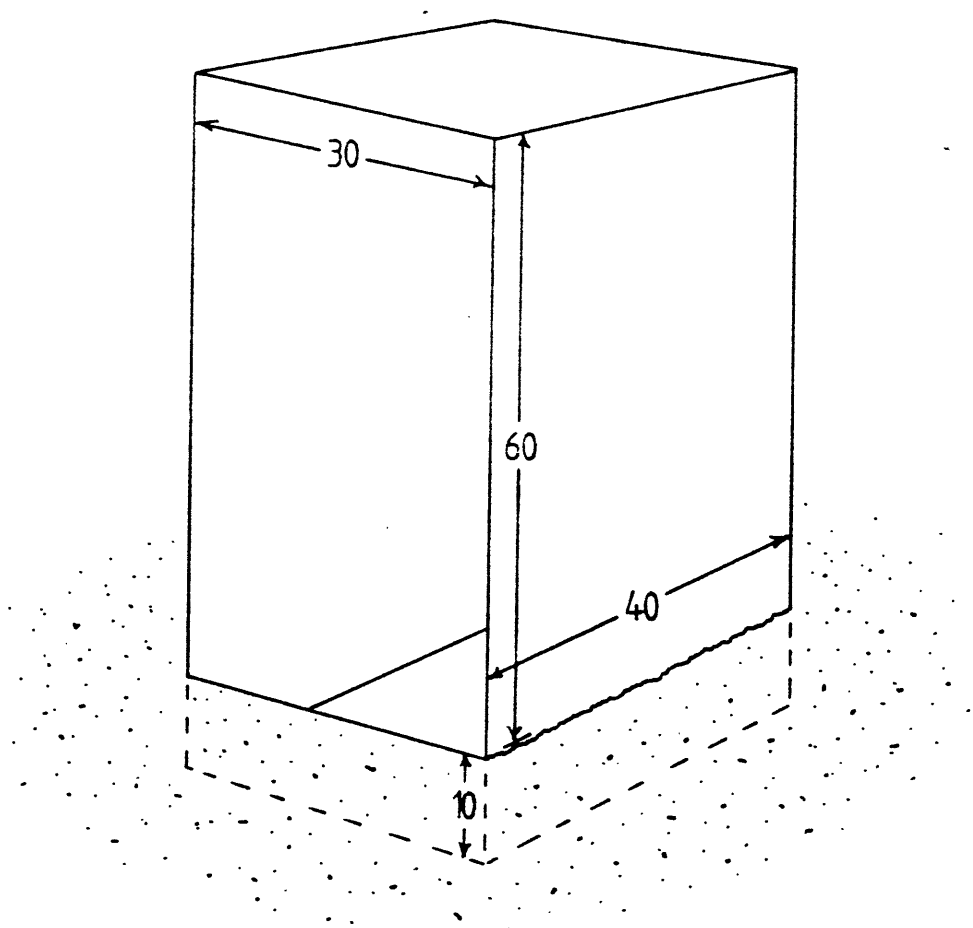

FIGURE 7.3: *Modified Bollinne splash trap. Dimensions in cm.*

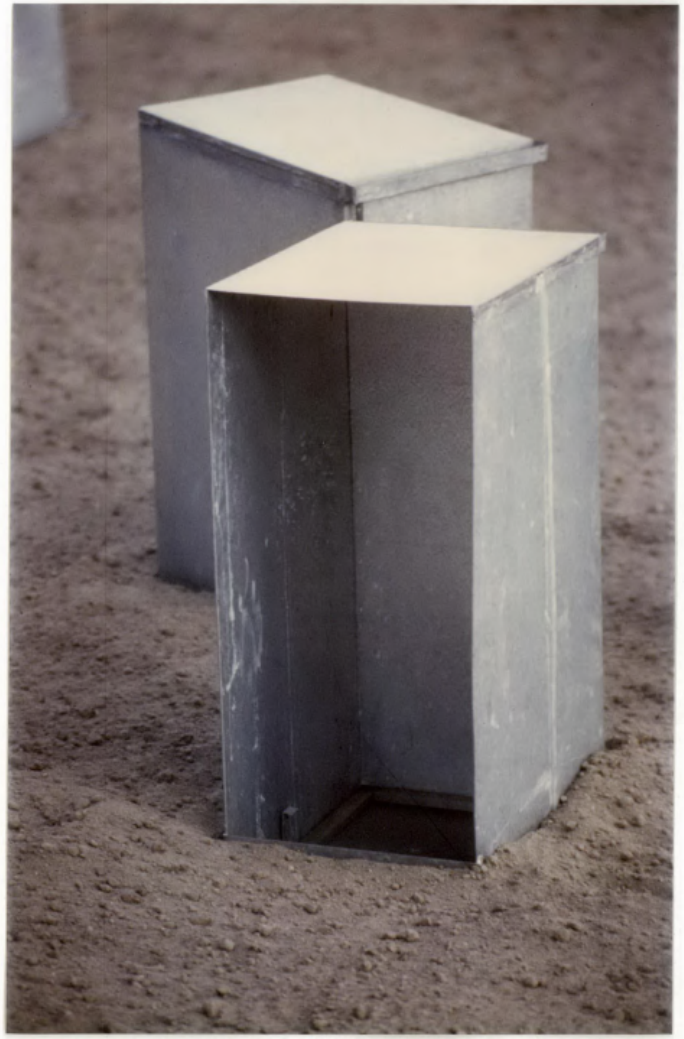

PLATE 7.3: *Modified Bollinne splash trap - dimensions given in Figure 7.3, page 135.*

PLATE 7.4: *Pipe splash trap - dimensions given in Figure 7.4, preceding page.*

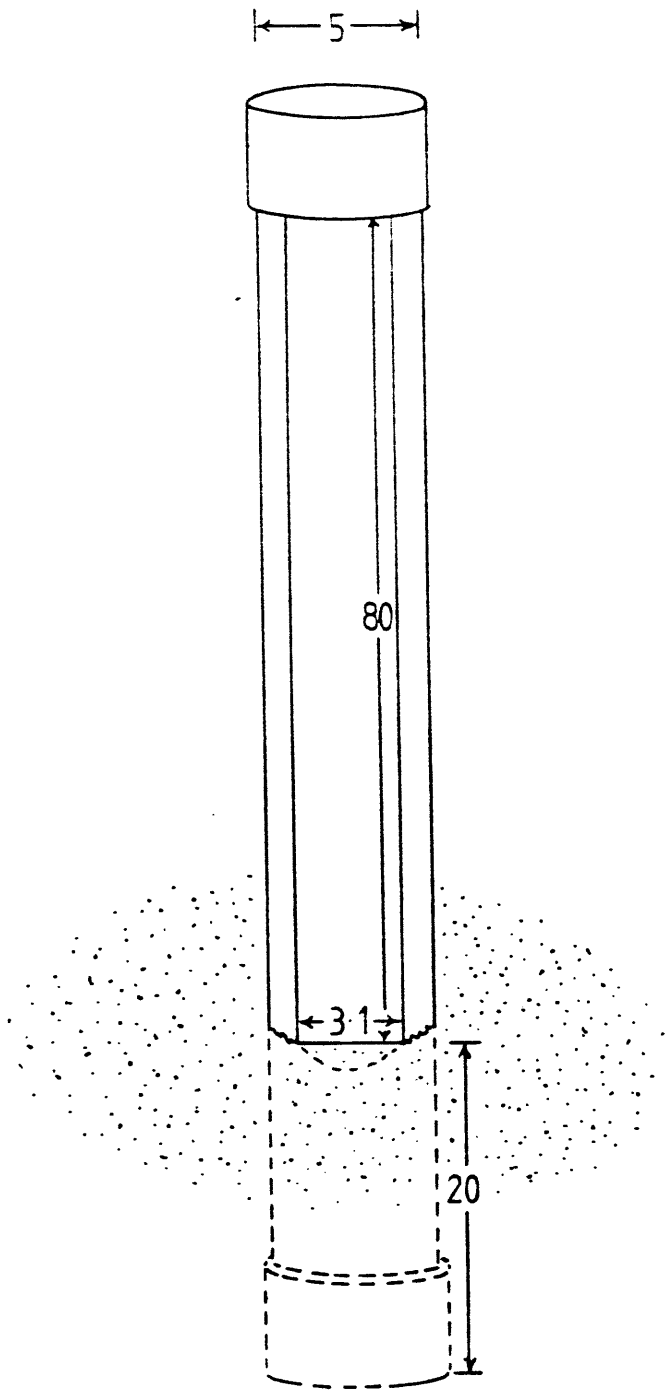

FIGURE 7.4: *Pipe splash trap. Dimensions in cm.*

based on an equilateral triangle of side 1.2 m with one trap at each corner facing in to the centre. The aperture of one trap of the three faced upslope. The arrays of the various types of splash trap were separated by at least 1.5 m. A general view of the splash trap layout is shown in Plate 7.5.

7.3.4 Supplementary instrumentation

A directional rain-gauge of the type described by Rose and Fairbrother (1960) was situated adjacent to the plot. This was read after each erosion event. A weather station recording windspeed and direction, and rainfall at six minute intervals was situated 200 m from the plot. Daily read rain-gauge records from this station were also available.

7.3.5 Procedure

The splash traps were set into the soil in the arrays described in Section 7.3.3. This involved excavation of a hole slightly larger than the portion of the trap to be buried, setting the trap in place, and filling the gap surrounding the splash trap. The splash traps were oriented by sighting with a prismatic compass. Particular attention was paid to ensuring that the soil area within splashing distance of the aperture or intercepting surface was in a similar condition for all splash traps. This was achieved by careful raking after the traps had been set in place and orientated. After each rainfall event, the traps were removed and the collected splash washed into plastic bottles, then transferred in the laboratory for oven drying and weighing.

7.3.6 Calculations

In accordance with the theory developed in Chapters 4 and 5, the mass collected by a splash trap, and adjusted for trap width, was taken as the component splash transport in the direction appropriate to the orientation of the particular trap. Each array measured three or four components, and the vector sum of these was taken as the resultant splash transport for the event.

PLATE 7.5: *Splash erosion plot at Newholme Field Laboratory. From left to right - directional rain gauge, two splash board array, four pipe trap array with three pipe trap array behind it, three modified Bollinne trap array. Meteorological station behind white fence in the middle distance.*

7.4 Tracer Study

This was also carried out at the plot used for the splash trap study. The marked soil was prepared by separating by sieving a sample of the sandy loam from the plot into fractions of particle size greater than, and less than 0.3 mm. As fluorescent paints were unobtainable at the time of the study, coloured spray-on enamels were used for marking. It was found possible to mark only the fraction with particle sizes greater than 0.3 mm, as particles smaller than this become glued into aggregates by the enamel. After light spray-painting and drying, the >0.3 mm fraction was recombined with the <0.3 mm fraction, the intention being to compare measurements of the transport of the >0.3 mm fractions from the tracer method and from the splash trap methods. At the plot site, a 5 cm length of 5 cm diameter p.v.c. pipe was pressed into the soil and the soil within removed. The soil with the >0.3 mm fraction painted was placed within the cylinder flush with the outside soil surface and the cylinder removed. After a rainfall event, soil cores of 1.5 cm diameter and 1 cm depth were removed along lines radiating from the pre-event tracer placement in upslope, downslope and left and right cross-slope directions. Cores were taken at distances from pre-event tracer placement of 4, 8, 12, 16, 20, 25, 30, 40, 50, 60 and 80 cm along each line. Taking of such shallow cores was greatly facilitated by the crusting nature of the soil. The soil from the cores was air dried and examined under a binocular microscope at X20 magnification, with a view to using a traversing stage to point-count the percentage of marked particles present in the sample.